applied sciences

MDPI

Article

An Unbalance Optimization Method for a Multi-Stage Rotor Based on an Assembly Error Propagation Model

Yue Chen [1,2], Jiwen Cui [1,2,*] and Xun Sun [1,2]

[1] Centre of Ultra-Precision Optoelectronic Instrument Engineering, Harbin Institute of Technology, Harbin 150080, China; 17b301001@stu.hit.edu.cn (Y.C.); 18b901005@stu.hit.edu.cn (X.S.)
[2] Key Lab of Ultra-Precision Intelligent Instrumentation, Harbin Institute of Technology, Ministry of Industry and Information Technology, Harbin 150080, China
* Correspondence: cuijiwen@hit.edu.cn; Tel.: +86-0451-8641-2041

Abstract: For the assembly of a multi-stage rotor, such as an aero-engine or gas turbine, the parts need to be assembled optimally to avoid excessive unbalance. We propose a method to optimize the unbalance of a multi-stage rotor during assembly. First, we developed an assembly error propagation model for a multi-stage rotor. The alignment process and distribution of the screw holes of the adjacent rotors was considered for the first time. Secondly, we propose a new assembly datum for unbalance optimization to ensure consistency with the actual conditions of a dynamic balance test. Finally, the unbalance optimization of a multi-stage rotor was achieved using a genetic algorithm, and the corresponding optimal assembly orientations of rotors at different stages were also identified. The results of the simulations showed that the assembly error propagation model had high accuracy and that the genetic optimization process had good convergence. The effect of unbalance optimization was also proven with experiments.

Keywords: error propagation model; assembly of multi-stage rotor; assembly datum; assembly optimization; rotor unbalance

Citation: Chen, Y.; Cui, J.; Sun, X. An Unbalance Optimization Method for a Multi-Stage Rotor Based on an Assembly Error Propagation Model. *Appl. Sci.* **2021**, *11*, 887. https://doi.org/10.3390/app11020887

Received: 1 December 2020
Accepted: 15 January 2021
Published: 19 January 2021

1. Introduction

The core components of rotating machinery, such as the high-pressure compressor of an aero-engine, are typically assembled by several single-stage rotors [1–3]. The machining errors of a single-stage rotor will propagate and accumulate during the assembly, which makes the actual assembly location of the rotor deviate from its ideal design location and the center of mass of the rotor deviate from the central inertia principal axis of the assembly, resulting in unbalance [4,5]. The unbalance caused by improper assembly is the main reason for vibration faults of rotating machinery.

The traditional way to eliminate unbalance is to measure the unbalance of the rotor with a dynamic balancing machine and then grind the rotor on a pre-set balanced surface [6,7]. This often requires repeated test runs and repairs to ensure the rotor meets the vibration requirements. This method not only costs time but also changes the initial unbalance of the single-stage rotor with the balanced surfaces. If the multi-stage rotor is reassembled, the unbalance of the single-stage rotor with balanced surfaces should be measured again. Therefore, there is an urgent need for an assembly optimization method that can not only predict the cumulative error of a multi-stage rotor after assembly but also achieve optimal matching of the assembly orientations of rotors at different stages to improve the assembly efficiency and one-time assembly qualified rate of multi-stage rotors.

The assembly optimization method of multi-stage rotors has been derived in many studies seeking to minimize the assembly cumulative errors. Hussain et al. [8] proposed an assembly error propagation model for 2-D rotational parts. For the first time, they came up with a strategy of straight-build assembly. To be specific, the line of centers of rotors at diverse stages can be as straight as possible by altering the assembly orientations of

these rotors. In [9], five assembly optimization methods were evaluated to reduce the error build-up in a straight-build assembly of 2D rectangular components.

Yang et al. [10] proposed another strategy of a parallelism-build assembly based on the above 2-D error propagation model. In line with such a strategy, the angular error between the actual and nominal mounting surfaces was minimized for the last-stage rotor. Such a 2-D error propagation model was further modified into a 3-D model by Yang et al. [11]. Then, they assumed that the key dimensions of rotors at various stages obeyed a normal distribution within a specified tolerance zone, and the eccentricity error of assembled rotors were predicted by tolerance analysis.

Hussain et al. [12] derived a progressive eccentricity error optimization model, and the corresponding physical significance still conformed to the concept of a straight-build assembly. Yang et al. [13] also probed into how the number of the circumferential assembly orientations affects the cumulative error of assembly. By constructing a probability density function of cumulative eccentric error of the last-stage rotor, Yang et al. [14] compared the global optimization results obtained by probability and the Monte Carlo method.

Jin et al. [15] proposed a solution to partial parallel chains for error analysis in aero-engine assembly. Sun et al. [16] proposed a neural network model for predicting the concentricity and perpendicularity of a multi-stage rotor. Depending on the location and orientation tolerance of rotor parts, an assembly error propagation model of a multi-stage rotor was constructed by Wang et al. [17] to achieve the optimal assembly orientations of rotors at different stages. Sun et al. [18] also derived the same error propagation model according to the coordinate propagation principle, which can provide guidance for the maintenance of aero-engines.

In all the above studies, the optimization objectives and known conditions all focused on the geometric attributes of rotors. The optimization of a rotor's mass attributes should be especially highlighted to prevent the vibrations of a multi-stage rotor from exceeding its upper limits. Piskin et al. [19] proposed a novel turbine balancing method using an Ant Colony algorithm. To optimize rotor unbalance, an assembly method was put forward by Liu et al. [20]. However, the center-of-mass coordinate in this study was not obtained by actual measurement but estimated by assuming a conversion ratio and based on the centroid coordinates. To overcome this defect, Sun et al. [21] made use of a vertical dynamic balancing machine to measure the mass attributes of rotors at different stages; on this basis, an assembly approach was proposed for the purpose of optimizing both the coaxiality and unbalance of rotors.

It can be seen from the current studies that an accurate error propagation model is very important for the prediction of assembly cumulative error and the guidance of the assembly process. The existing error propagation models were derived based on the axisymmetric characteristics of the rotating body and combined with coordinate propagation theories; however, the alignment processes and distribution of the screw holes around the rotors at different stages were ignored, and the selection of assembly orientations should be discrete.

The above problems are not clearly specified in the existing assembly optimization methods. When optimizing the rotor unbalance, the selection of the assembly datum should not be the same as that of the coaxiality optimization but should be consistent with the actual rotating axis of the dynamic balance test.

Targeted at the above problems, an unbalance optimization method of a multi-stage rotor is proposed in this study. In Section 2.1, an assembly error propagation model is developed, and the alignment processes and distribution of screw holes of adjacent rotors are introduced into the model. In Section 2.2, a new assembly datum for unbalance optimization of multi-stage rotor is calculated to ensure that the optimization datum and the measurement datum is truly realized. In Section 2.3, the unbalance optimization of a multi-stage rotor is achieved using a genetic algorithm (GA). In Section 3.1, the calculated accuracy of the assembly error propagation model is validated, and the optimization performance of GA is presented in Section 3.2. Finally, in Section 4, the effect of the unbalance optimization is proven in experiments.

2. Methods

2.1. Assembly Error Propagation Model

Limited to the current industrial level, the geometric deviations of the single-stage rotor are inevitable in the process of machining. The concentricity and parallelism errors of the assembly mounting surfaces of rotors at different stages are propagated stage by stage continuously, forming assembly cumulative errors. In Figure 1, the initial state of a 3-D two-stage simulation rotor before assembly is portrayed. Clearly, when the bottom mounting surface of each single-stage rotor is selected as the measurement datum, P_1 refers to a parallelism error of the top mounting surface of Rotor 1, P_2 to that of the top mounting surface of Rotor 2, and C_1 and C_2 are the concentricity errors of Rotor 1 and Rotor 2, respectively.

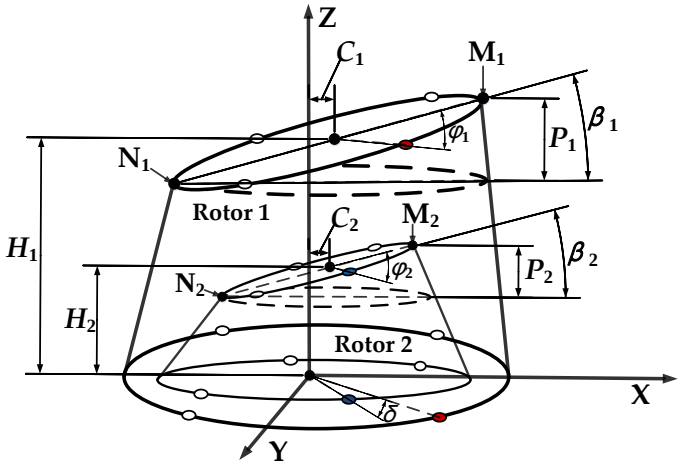

Figure 1. The initial state of a 3-D two-stage simulation rotor before assembly.

A pair of screw holes is randomly selected in the circumferential direction of the rotor for calibration, and the sampling angle of the highest point of the top mounting surface is recorded with the center of the calibrated screw hole as the sampling starting point. The red and blue dots in Figure 1 are the calibrated screw holes of Rotor 1 and Rotor 2, respectively. M_1 and M_2 are the highest points of the top mounting surface of Rotor 1 and Rotor 2, respectively. N_1 and N_2 are the lowest points of the top mounting surface of Rotor 1 and Rotor 2, respectively.

In Figure 1, the bottom mounting surface of Rotor 1 is used as an XY plane, and the normal axis passing through it is taken as the Z axis. The X axis is formed by a projection axis on the bottom surface of a line connecting the highest and the lowest points of the top mounting surface of Rotor 1. δ refers to the phase difference between the calibrated screw holes of Rotor 1 and Rotor 2. After that, the assembly process of the two-stage rotor can be divided into the following four steps (see Figure 2):

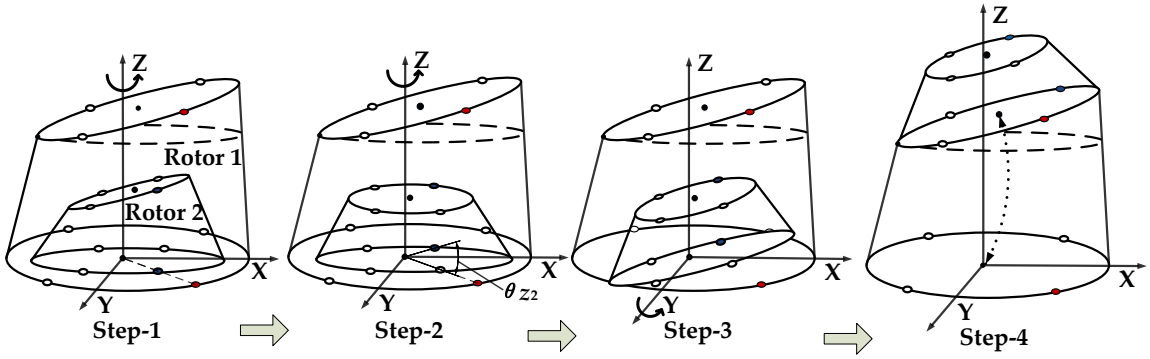

Figure 2. The assembly processes of a 3-D two-stage simulation rotor.

Step-1: Alignment of the calibrated screw holes.

In actual assembly, the screw holes of Rotor 1 and Rotor 2 must be aligned first (i.e., Rotor 2 rotates an angle of δ around the axis Z relative to Rotor 1), and then the assembly orientation can be selected with this state as the initial state. Although the angle of δ cannot be determined, the phase difference $(\varphi_2 - \varphi_1)$ between the highest points of Rotor 1 and Rotor 2 after assembly can be obtained by measuring the sampling angle between the calibrated screw hole and its highest point of each stage rotor.

Step-2: Selection of the optimal assembly orientation.

Assuming that Rotor 1 is fixed, the calibrated screw holes of Rotor 2 and Rotor 1 must be aligned first. This is the initial state to select the appropriate assembly orientation of Rotor 2, and the rotation matrix of Rotor 2 relative to Rotor 1 about the Z axis can be expressed as follows:

$$Rz_2 = \begin{bmatrix} \cos[\theta z_2 + (\varphi_2 - \varphi_1)] & -\sin[\theta z_2 + (\varphi_2 - \varphi_1)] & 0 \\ \sin[\theta z_2 + (\varphi_2 - \varphi_1)] & \cos[\theta z_2 + (\varphi_2 - \varphi_1)] & 0 \\ 0 & 0 & 1 \end{bmatrix} \quad (1)$$

where θz_2 refers to an angle by which Rotor 2 rotates around the Z axis relative to Rotor 1, φ_2 refers to an angle between the center of the calibrated screw hole of Rotor 2 and its highest point, and φ_1 to that of Rotor 1. $(\varphi_2 - \varphi_1)$ refers to the phase difference between the highest point of Rotor 2 and that of Rotor 1 after alignment of the calibrated screw holes of Rotor 2 and Rotor 1. Considering the discrete and uniform distribution of the screw holes, the selection range of θz_2 was $0{-}180^\circ$, and the optional angle was $q(180/k)$, where k is the number of circumferential screw holes on the mounting surface, and q represents how many distribution angles the calibrated screw hole needs to rotate.

Step-3: Rotation.

Rotor 2 is rotated by an angle of β_2 around the Y axis so that the bottom mounting surface of Rotor 2 is parallel to the top mounting surface of Rotor 1. Then the rotation matrix of Rotor 2 relative to Rotor 1 about the Y axis can be expressed as follows:

$$Ry_2 = \begin{bmatrix} \cos(\beta_2) & 0 & \sin(\beta_2) \\ 0 & 1 & 0 \\ -\sin(\beta_2) & 0 & \cos(\beta_2) \end{bmatrix} \quad (2)$$

where β_2 is an angle formed by the top and bottom mounting surfaces of Rotor 2 and can be calculated as follows:

$$\beta_2 = \arctan\left(\frac{P_2}{2D_2}\right) \quad (3)$$

where D_2 is the measured radius of the top mounting surface of Rotor 2.

Step-4: Translation.

Rotor 2 is translated so that the center of the bottom mounting surface of Rotor 2 coincides with the top mounting surface of Rotor 1, which is equivalent to directly accumulating the center coordinates of the top mounting surface of Rotor 1 on the basis of Step-2.

Through the above steps, the assembly error propagation model of a 2-stage rotor can be expressed as follows:

$$X_2 = I_2 Rz_2 Ry_2 + S_1 \quad (4)$$

where X_2 refers to a coordinate vector of any point in Rotor 2 after assembly, and I_2 to that in Rotor 2 before assembly. Rotor 1 does not move by default, and S_1 is the coordinate vector of the center of the top mounting surface of Rotor 1.

The assembly process of an n-stage rotor can be regarded as the assembly processes of $(n-1)$ two-stage rotor. Therefore, the assembly error propagation model of an n-stage rotor can be expressed as follows:

$$X_n = I_n \left[\prod_{n:-1:1} (Rz_n Ry_n) \right] + S_1 (n \in N^*, n>1) \tag{5}$$

where X_n refers to a coordinate vector of any point in rotor n after assembly, I_n to that in rotor n before assembly, Rz_n to a rotation matrix of rotor n relative to rotor $(n-1)$ about the Z axis, and Ry_n to a rotation matrix of rotor n relative to rotor $(n-1)$ about the Y axis.

For a rigid rotor, the coordinate vector of any point in rotors at different stages before and after assembly can be accurately predicted by Equation (5) on the premise that the geometric errors of rotors at different stages are known. The parameters needed to solve Equation (5) include concentricity (C_n), parallelism (P_n), measured radius (D_n), the angle between the calibrated screw hole and the highest point (φ_n), and the height of mounting surface (H_n), which can be obtained using a coordinate measuring instrument (CMM); only θz_n is unknown and is to be optimized.

2.2. Assembly Datum for Unbalance Optimization

The mathematical definition of unbalance is the product of the mass of a rotor and the eccentricity error of the center of mass and can also be expressed as the product of an unbalanced mass block and its effect radius. During the dynamic balance test of a rotor, journals of the front and back shafts of the rotor are respectively positioned on the support frames on left and right sides of a dynamic balancing machine.

The axis of rotation should be approximately the central line between the journals of the front and back shafts, and the measured vector radius of the mass eccentricity should be perpendicular to such an axis of rotation (i.e., the orientation-varying axis in Figure 3). This axis of rotation will vary along with variations in the assembly orientations of rotors at different stages. For the optimization of the rotor unbalance, this axis of rotation should be used as the assembly datum. The unbalance of rotors at different stages after assembly can be obtained as follows:

$$U_n = m_n r'_n, \tag{6}$$

where U_n is the unbalance of rotor n after assembly, that is a product of m_n (unbalanced mass) and $r_n{}'$ (i.e., the vector of the effect radius of rotor n). As for $r_n{}'$, it can be solved by the following steps:

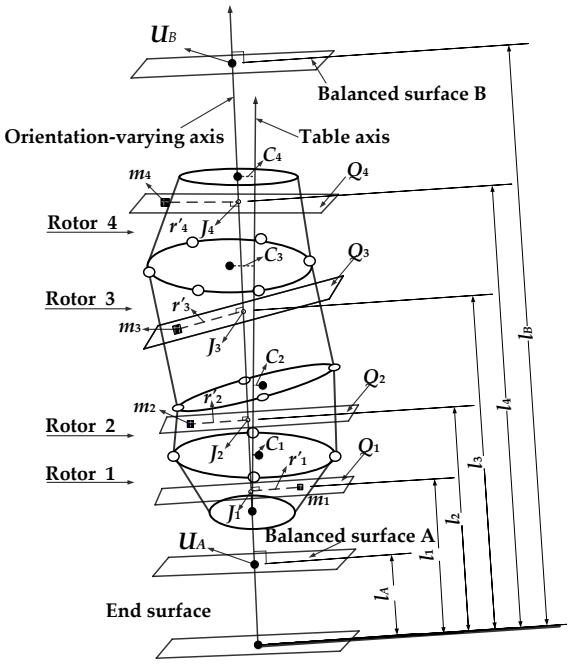

Figure 3. Assembly datum for unbalance optimization of four-stage rotor.

Step-1: A linear equation expressing the orientation-varying axis can be written as follows:

$$\frac{x - x_0}{e'_{nx} - x_0} = \frac{y - y_0}{e'_{ny} - y_0} = \frac{z - z_0}{e'_{nz} - z_0} = t_n, \tag{7}$$

where (x_0, y_0, z_0) is a coordinate vector of the bottom center of the bottom rotor. Under the circumstance that the table axis serves as the datum for measurement of the rotor's geometric parameters, such a point is the origin of the coordinates by default.

Step-2: As for the plane Q_n that is extended across an unbalanced mass point of rotor n and perpendicular to the orientation-varying axis, it is expressed in the equation below:

$$\begin{cases} (e'_{nx} - x_0)(x - r'_{nx}) + (e'_{ny} - y_0)(y - r'_{ny}) + (e'_{nz} - z_0)(z - r'_{nz}) = 0 \\ (R'_n = \begin{bmatrix} r'_{nx} & r'_{ny} & r'_{nz} \end{bmatrix}, R_n = \begin{bmatrix} r_{nx} & r_{ny} & r_{nz} \end{bmatrix}) \end{cases}, \tag{8}$$

where $R_n{}'$ refers to a coordinate vector of the unbalanced mass point of rotor n after assembly. R_n refers to the initial coordinate vector of the unbalanced mass point of rotor n before assembly, and it can be measured by the dynamic balancing machine or artificially added. By substituting R_n into Equation (5), $R_n{}'$ is solved.

Step-3: Coordinates of an intersecting point between the orientation-varying axis and the plane Q_n are expressed as follows:

First, Equations (7) and (8) form a simultaneous equation. Through such a simultaneous equation, parameter t_n in the linear equation expressing the orientation-varying axis can be obtained:

$$t_n = \frac{(e'_{nx} - x_0)(r'_{nx} - x_0) + (e'_{ny} - y_0)(r'_{ny} - y_0) + (e'_{nz} - z_0)(r'_{nz} - z_0)}{(e'_{nx} - x_0)^2 + (e'_{ny} - y_0)^2 + (e'_{nz} - z_0)^2}. \tag{9}$$

By substituting t_n into Equation (7), the coordinates of the intersection point Jn can be acquired.

Step-4: The effect radius of the unbalanced mass relative to the orientation-varying axis, that is the modulus of, $r_n{}'$, is expressed in the following equation:

$$r'_n = \sqrt{(j_{nx} - r'_{nx})^2 + (j_{ny} - r'_{ny})^2 + (j_{nz} - r'_{nz})^2} (J_n = \begin{bmatrix} j_{nx} & j_{ny} & j_{nz} \end{bmatrix}). \tag{10}$$

By substituting Equation (10) into Equation (6), a value of U_n is acquired. After that, the unbalance of rotors at diverse stages should be decomposed to the balanced surfaces A and B through Equation (11):

$$\begin{cases} U_A = \sum_{j=1}^{n} \frac{l_B - l_j}{l_B - l_A} U_j \\ U_B = \sum_{j=1}^{n} \frac{l_j - l_A}{l_B - l_A} U_j \end{cases}, \tag{11}$$

where U_A and U_B turn out to be the unbalance of an n-stage rotor on the balanced Surfaces A and B, respectively. l_A and l_B are the distances between the balanced Surfaces A and B from the support point of the journal, respectively. l_j is the distance between the unbalanced measuring surface of each rotor and the balanced Surface A. In this context, the maximum unbalance of the n-stage rotor can be obtained by the following equation:

$$U = \max(U_A, U_B). \tag{12}$$

2.3. Genetic Optimization Algorithm

As a global optimization algorithm, genetic algorithms (GA) are aimed at mapping the solution space to a genetic space, encoding each set of possible solutions into a chromosome. First, a series of candidate solutions are randomly generated, and they form an initial population. Based on a fitness function designed in advance according to the

objective function, the fitness of each individual to the problem solving environment is calculated. Then, corresponding selections are made in consistency with the obtained fitness, suppressing chromosomes with low fitness, but promoting those with high fitness.

After that, genetic manipulations, such as crossovers and mutations are performed for the purpose of evolving the next-generation population. Through repeated operations as described above, constant evolution toward optimized solutions is achieved. At last, except for a population that meets the corresponding convergence conditions and is the most adaptive to the problem solving environment, the optimal solution is also obtained. Depending on the above thoughts of genetic optimization, a GA fitness function of the unbalance of an n-stage rotor can be expressed as follows:

$$\begin{cases} fitness\_U(x) = U(x) \\ \text{s.t} \quad x = (\theta_{z1}, \theta_{z2}, \ldots\ldots, \theta_{zn}), 0 \le \theta_{zn} \le 180^\circ \end{cases}, \tag{13}$$

where design variable x represents a vector formed by assembly orientations of the n-stage rotor. In terms of GA, its steps are detailed below:

Step-1 (initial population): the n elements in an assembly orientation sequence x are regarded as n genes; and each gene varies from 0° to 180°. Each chromosome is composed of n genes. In this way, 1000 chromosomes are randomly generated and act as an initial population.

Step-2 (individual evaluation): the fitness of each chromosome is determined for individual evaluation.

Step-3 (selection): chromosomes with the optimal fitness are selected and take the place of a chromosome of the worst fitness.

Step-4 (mutation): the purpose of mutation is to improve the current chromosome. According to Equation (14), the chromosome with higher fitness has a smaller variation range. As for chromosomes with lower fitness, their variation ranges are larger accordingly.

$$x_{new} = x\left[1 \pm \gamma\left(1 - \frac{f}{f_{best}}\right)^2\right], \tag{14}$$

where x_{new} and x are chromosomes after/before mutation respectively. γ is a random number between 0 and 1, and f stands for the fitness of x, while f_{best} stands for the optimal fitness of the present population.

Step-5 (crossover): some genes are randomly selected from two chromosomes for replacement and recombination. In this way, a new chromosome is generated. By means of crossover, the search capability of the GA can be enhanced.

Step-6 (termination criteria): the algorithm is ended when the fitness of optimal individuals and the population ceases to rise and the number of iterations reaches the designed value.

3. Simulation

3.1. Validation of Assembly Error Propagation Model

In Section 2.1, an assembly error propagation model of a multi-stage rotor was developed to predict the changes of coordinate values of any point in each rotor before and after assembly on the premise that the geometric parameters of rotors at different stages are known. To verify the calculated accuracy of the assembly error propagation model, the geometric parameters of a three-stage rotor presented in [17] (see Table 1) are used for reference for a simulation. In addition, the angle between the calibrated screw holes and the highest points is 0° by default (i.e., $\varphi_1 = \varphi_2 = \varphi_3 = 0^\circ$). The assembly orientations of the first rotor, second rotor, and third rotor were set to 0°, 30°, and 60° respectively (i.e., $\theta z_1 = 0^\circ$; $\theta z_2 = 30^\circ$; and $\theta z_3 = 60^\circ$).

The new coordinates of the center of the top mounting surface of the second and the third stage rotors after assembly were calculated using the model. SolidWorks, a 3-D software for drawing, was utilized to reconstruct the corresponding three-stage rotor model.

Through a measurement function of the software, the coordinates of the center of the top mounting surface of the assembled rotors at different stages were measured (see Figure 4). As shown in Table 2, the calculated results achieved by the model are in good agreement with those measured by the software.

Table 1. The geometric parameters of the three-stage rotor [17].

Stage	Height (H_n) [mm]	Measured Radius (D_n) [mm]	Concentricity (C_n) [mm]	Parallelism (P_n) [mm]	Sampling Angle (φ_n) [°]
1	70	100	0.005	0.005	0
2	70	100	0.005	0.005	0
3	70	100	0.005	0.005	0

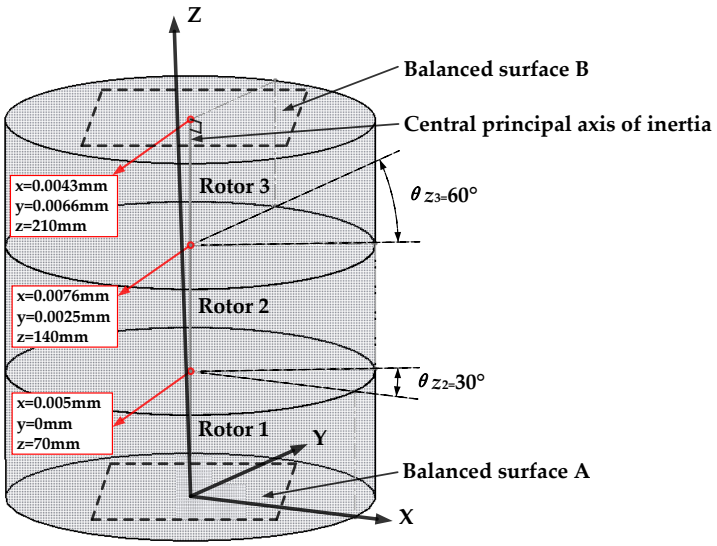

Figure 4. The center coordinates of the top mounting surface of the assembled three-stage rotor were measured using software.

Table 2. The center coordinates of the top mounting surface of the assembled three-stage rotor.

Stage	Calculated Results [mm]	Measured Results [mm]
1	(0.005, 0, 70)	(0.005, 0, 70)
2	(0.0076, 0.0025, 140)	(0.0076, 0.0025, 140)
3	(0.0043, 0.0066, 210)	(0.0043, 0.0066, 210)

3.2. GA-Based Unbalance Optimization

We assumed that the three-stage simulation rotor described in Section 3.1 is made of steel. The initial coordinates of the center of mass of the rotors at different stages were measured using software (see Table 3). The initial unbalance of each rotor is the product of its mass and the vertical distance from the center of mass to the central inertia principal axis, which can be obtained using Equation (6). As shown in Figure 4, the balanced Surfaces A and B of the three-stage rotor are perpendicular to the central principal axis of inertia (i.e., the line connecting the center of the top mounting surface and the bottom surface) and, respectively, pass through the center of the top mounting surface and the bottom surface.

l_A is set as 0, and l_B is equal to the distance between the center of the top and bottom mounting surfaces of the three-stage rotor. The unbalance on the balanced Surfaces A and B can be obtained by Equation (11), and the integral unbalance of the three-stage rotor can be obtained by Equation (12). The minimum and maximum unbalance are

taken as the optimization objectives, and the genetic algorithm proposed in Section 2.3 is applied to calculate the optimal assembly orientations of the second and third stage rotors. In terms of the first stage rotor, its assembly orientation was designed at 0° by default; each chromosome was designed to hold two genes, that is (θz_2, θz_3); and, the number of initial populations was set at 1000.

Table 3. The mass parameters of the three-stage rotor measured using software.

Stage	Mass [kg]	Initial Coordinates of the Center of Mass [mm]
1	17.2630	(0.0036, 0, 35)
2	17.2630	(0.0036, 0, 35)
3	17.2630	(0.0036, 0, 35)

In addition, the selection principle of the internal parameters of the GA referred to the literature [22], and the mutation rate, crossover rate, and iterative times were set as 0.01, 0.9, and 500, respectively. The convergence progress of the GA-based unbalance optimization of the three-stage rotor is shown in Figure 5. When θz_2 and θz_3 were 0° and 180°, respectively, the corresponding minimum unbalance reached 32.2568 g·mm (minimum unbalance), as shown in Table 4. When θz_2 and θz_3 were 180° and 180°, respectively, the corresponding maximum unbalance reached 129.6123 g·mm (maximum unbalance).

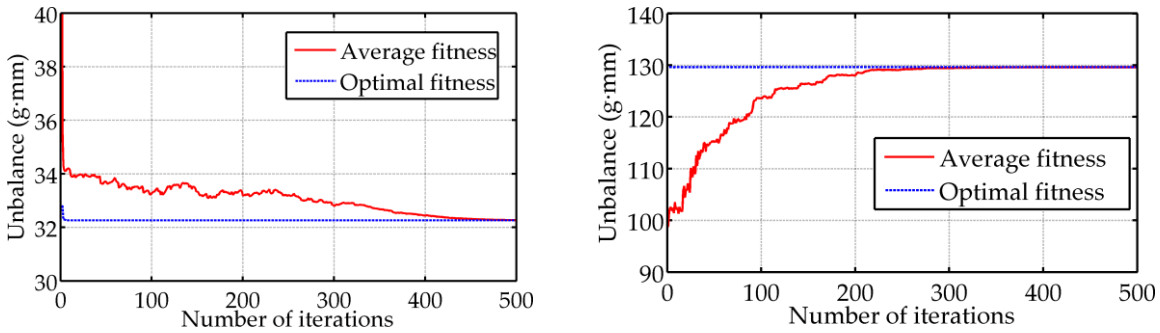

(**a**) (**b**)

Figure 5. The convergence progress of the genetic algorithm (GA)-based unbalance optimization. (**a**) Taking the minimum unbalance as the optimization objective. (**b**) Taking the maximum unbalance as the optimization objective.

Table 4. Results of the GA-based unbalance optimization.

Optimization Objective	θz_1 [°]	θz_2 [°]	θz_3 [°]	Unbalance [g·mm]
Minimum unbalance	0	0	180	32.2568
Maximum unbalance	0	180	180	129.6123

Further considering the distribution of the assembly screw holes, the optional assembly orientations of the rotors at different stage are discrete, and the optimal corresponding relationship of the screw holes of the rotors should be obtained by a secondary calculation according to the above optimal solution. As shown in Figure 6, assuming the optimal orientation obtained by the optimization is θ, θ_1 and θ_2 are the two optional orientations adjacent the optimal orientation. The fitness in both cases must be calculated again, and the optimal solution can be selected. The angles of the screw holes adjacent to the optimal solution were determined by calculating all possible alignment relations (number: 2^{n-1}) for n-stage rotors.

As assumed, there were 24 circumferential screw holes on the top and bottom mounting surfaces of each rotor of the above three-stage simulation rotor; and the distributed angle of the screw holes was set at 15°. Since the optimal solution is exactly a multiple of the

distribution angle (15°), the minimum unbalance can be obtained when Rotor 2 rotates zero distributed angles (0 × 15 = 0°) relative to Rotor 1, and Rotor 3 rotates 12 distributed angles (12 × 15 = 180°) relative to Rotor 2. When Rotor 2 rotates 12 distributed angles (12 × 15 = 180°) relative to Rotor 1 and Rotor 3 rotates 12 distributed angles (12 × 15 = 180°) relative to Rotor 2, the unbalance of the assembly reaches the maximum value.

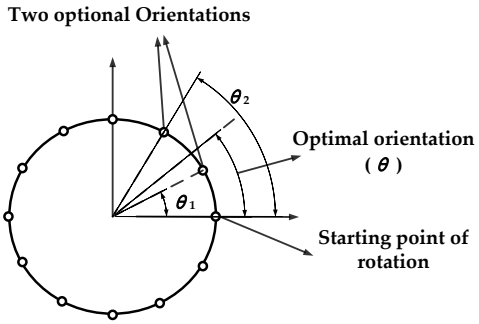

Figure 6. Selection of the optimal orientations between two optional orientations.

4. Experiments

An aero-engine was scaled in a certain proportion and simplified to a four-stage simulation rotor. A section view of the four-stage rotor is shown in Figure 7. As observed, it was composed of a front shaft, a low-pressure compressor (LPC), a high-pressure compressor (HPC), and a back shaft. Each single-stage rotor was assembled step by step through its own axial and radial front edge, and connected by a certain number of screws. The distances between the two pre-set balanced Surfaces A and B from the support point were l_A and l_B, respectively. To further prove the validity of the proposed assembly optimization method in this paper, experiments were performed, and the corresponding experimental steps are detailed below:

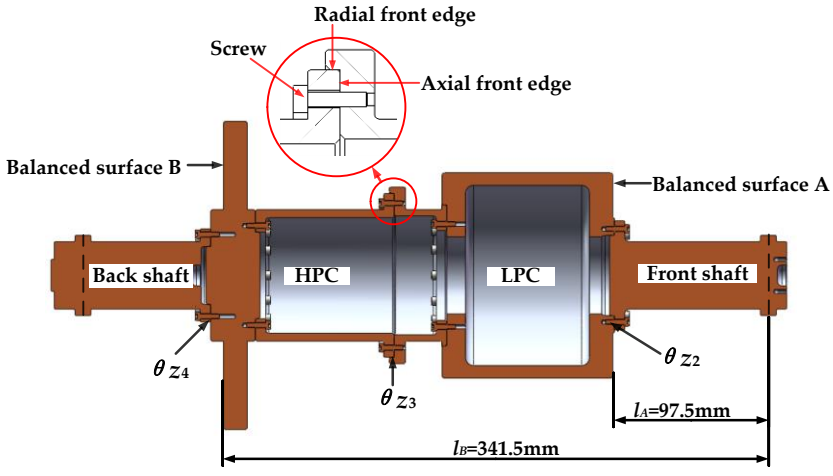

Figure 7. The section view of the four-stage rotor.

Step-1: The geometric parameters of the rotors at different stages were measured by a 3-D CMM.

Figure 8 shows the measured actual scene and schematic diagram of the HPC. First, the center of a pair of screw holes on the mounting surface of HPC was calibrated. Taking this center as the starting point of sampling, the concentricity (C_n), the parallelism (P_n), the measured radius (D_n), an angle between this center and the highest point (φ_n), and the high point (H) of the mounting surface of the HPC were measured successively. As shown in Figure 8b, the circle of diameter t_1 is the tolerance zone defined by the concen-

tricity specification, and the distance t_2 is the tolerance zone defined by the parallelism specification. The measuring principle of the LPC and front and back shaft was the same as that of the HPC. The geometric parameters of component of the four-stage rotor were measured by a 3-D CMM for six times, and presented in Tables 5–8, respectively. As shown in Table 9, the standard uncertainties of different measured parameters were calculated by the equation below:

$$u(x) = \sqrt{\frac{\sum_{i=1}^{n} (x_i - x_a)^2}{n(n-1)}}, \tag{15}$$

where n refers to the number of measurements, and x_a refers to the mean value of the six measurement results. The distributed numbers of the screw holes of rotors at different stages are shown in Table 10. The optimal assembly orientations of each rotor can only be selected from these discrete angles.

Table 5. The measured geometric parameters of the front shaft.

Sequence	C_n [mm]	P_n [mm]	D_n [mm]	φ_n [°]	H_n [mm]
1	0.0153	0.0130	50.0130	79	96.5410
2	0.0161	0.0147	50.0136	81	96.5425
3	0.0158	0.0110	50.0122	79	96.5480
4	0.0139	0.0123	50.0145	79	96.5438
5	0.0143	0.0128	50.0171	80	96.5450
6	0.0152	0.0131	50.0125	81	96.5422

Table 6. The measured geometric parameters of the low pressure compressor (LPC).

Scheme	C_n [mm]	P_n [mm]	D_n [mm]	φ_n [°]	H_n [mm]
1	0.0944	0.0235	101.0910	174	105.1940
2	0.0912	0.0194	101.0921	175	105.1915
3	0.0935	0.0200	101.0850	174	105.1970
4	0.0990	0.0223	101.0915	174	105.1984
5	0.0925	0.0219	101.0946	175	105.1960
6	0.0950	0.0231	101.0972	176	105.1921

Table 7. The measured geometric parameters of the high pressure compressor (HPC).

Sequence	C_n [mm]	P_n [mm]	D_n [mm]	φ_n [°]	H_n [mm]
1	0.0963	0.0151	36.0190	13	114.7130
2	0.0927	0.0143	36.0188	12	114.7189
3	0.0930	0.0148	36.0204	12	114.7205
4	0.0979	0.0167	36.0175	12	114.7150
5	0.0911	0.0156	36.0170	13	114.7137
6	0.0954	0.0152	36.0195	13	114.7118

Table 8. The measured geometric parameters of the back shaft.

Sequence	C_n [mm]	P_n [mm]	D_n [mm]	φ_n [°]	H_n [mm]
1	0.0496	0.0111	50.1200	210	80.2250
2	0.0485	0.0125	50.1225	210	80.2245
3	0.0501	0.0105	50.1238	211	80.2210
4	0.0512	0.0134	50.1150	211	80.2265
5	0.0495	0.0115	50.1220	211	80.2193
6	0.0490	0.0128	50.1231	212	80.2200

Table 9. The standard uncertainties of different measured parameters.

Component	$u(C_n)$ [μm]	$u(P_n)$ [μm]	$u(D_n)$ [μm]	$u(\varphi_n)$ [°]	$u(H_n)$ [μm]
Front shaft	0.35	0.49	0.74	0.40	1.02
LPC	1.10	0.68	1.67	0.33	1.13
HPC	1.04	0.33	0.52	0.22	1.41
Back shaft	0.38	0.45	0.32	0.31	1.22

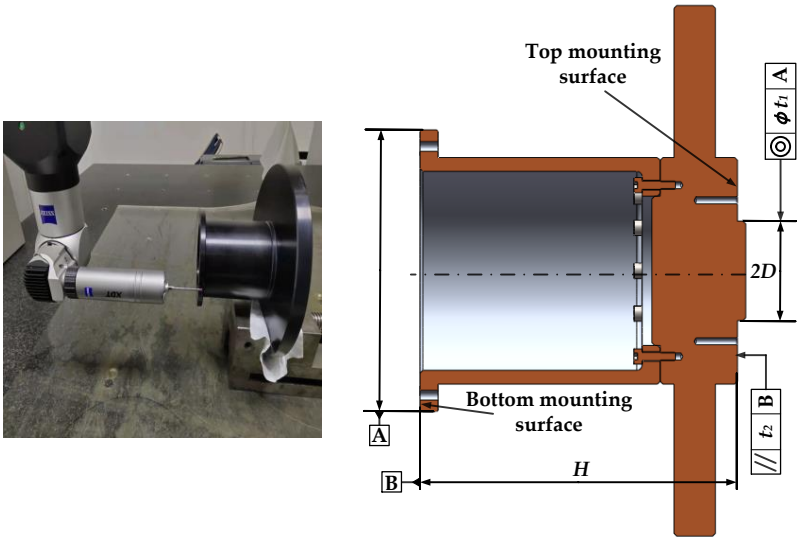

(**a**) (**b**)

Figure 8. Measurement of the geometric parameters of a high-pressure compressor (HPC). (**a**) Measured scene. (**b**) Schematic diagram.

Table 10. The distributed numbers of the screw holes of each component.

Component	Distributed Numbers (Top Mounting Surface)	Distributed Numbers (Bottom Mounting Surface)
Front shaft	12	12
LPC	24	12
HPC	12	24
Back shaft	12	12

Step-2: The initial unbalance of the four-stage rotor was artificially added to each rotor.

To better reflect the experimental effect of the unbalance optimization, the unbalanced mass was artificially added to the rotors at different stages, which is far greater than the unbalance caused by uneven material distribution. Hexagon-socket-head-screws were used for the connection of the four-stage rotor, as shown in Figure 9. The method was to replace an original M4 × 12-screw with a M4 × 20-screw at the calibrated screw hole of rotors at different stages to produce an unbalanced mass with a mass difference of about 2 g, whose effect radius and phase are known. The initial unbalance parameters of the four-stage rotor are shown in Table 11.

Table 11. The initial unbalance parameters of the four-stage rotor.

Component	Unbalanced Mass [G]	Phase Relative to Calibrated Screw Hole [°]	Effect Radius [Mm]	Axial Coordinate of The Unbalanced Mass Point Relative to Measured Datum [Mm]
Front shaft	2	0	58	96.5
LPC	2	0	64	105
HPC	2	0	90	0
Back shaft	2	0	51	0

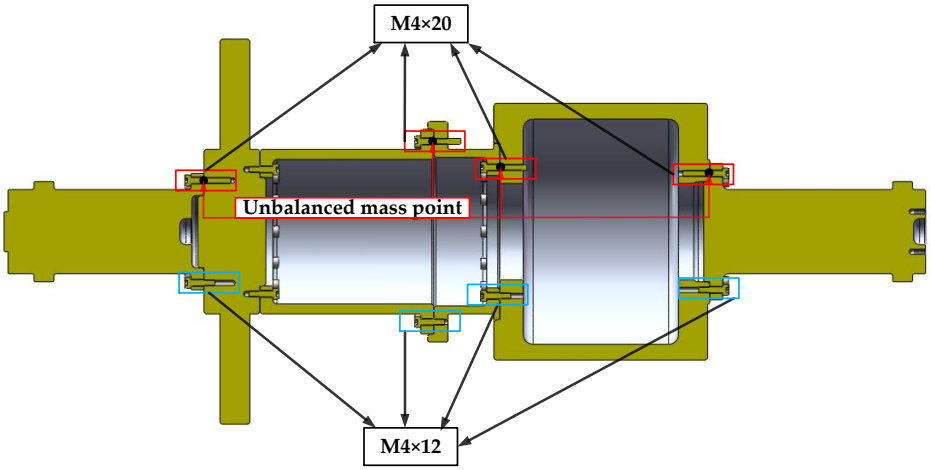

Figure 9. The setting of the initial unbalance of the four-stage rotor.

Step-3: The unbalance of the four-stage rotor was measured using a dynamic balancing machine.

According to the geometric and unbalance parameters obtained in Step-1 and Step-2, the genetic algorithm derived in Section 3.2 was used to calculate the optimal assembly orientations of the rotors at different stages with three assembly strategies as follows:

Strategy-1: the minimum unbalance was set as the optimization objective;

Strategy-2: the maximum unbalance was set as the optimization objective; and

Strategy-3: direct assembly (i.e., the rotors at each stage remained in their initial state).

The optimal assembly orientations of each component and the corresponding unbalance of the four-stage rotor were calculated according to Strategy-1, Strategy-2, and Strategy-3, respectively, as shown in Tables 12–14. θz_1, θz_2, θz_3, and θz_4 were the optimal assembly orientations of the front shaft, the LPC, the HPC, and the back shaft, respectively, without considering the distribution of the screw holes of each component. The mean value and standard deviations of the optimal results were provided in Table 15. Furthermore, the optimal assembly orientations where the screw hole exists were obtained by a secondary calculation. As shown in Table 16, the optimal assembly orientations achieved during six iterations were exactly same. This indicates that the measurement errors of each parameter had little influence on the optimal results, especially when considering the existence of the distributed screw holes of each component.

Table 12. The optimal results were calculated according to Strategy-1.

Sequence	θz_1 [°]	θz_2 [°]	θz_3 [°]	θz_4 [°]	Unbalance [g·mm]
1	0	120.01	116.03	123.00	181.15
2	0	120.00	118.04	122.00	180.90
3	0	120.04	117.04	121.00	182.46
4	0	120.00	117.04	121.00	182.50
5	0	120.01	117.03	122.00	181.53
6	0	120.01	118.04	121.00	181.60

Table 13. The optimal results were calculated according to Strategy-2.

Sequence	θz_1 [°]	θz_2 [°]	θz_3 [°]	θz_4 [°]	Unbalance [g·mm]
1	0	140.80	45.20	30.17	402.15
2	0	143.92	45.07	30.01	401.90
3	0	141.99	45.00	30.00	402.46
4	0	141.92	45.07	30.04	402.50
5	0	141.97	45.02	30.01	401.53
6	0	142.95	45.04	30.00	404.60

Table 14. The optimal results were calculated according to Strategy-3.

Sequence	θz_1 [°]	θz_2 [°]	θz_3 [°]	θz_4 [°]	Unbalance [g·mm]
1	0	0	0	0	324.60
2	0	0	0	0	328.13
3	0	0	0	0	324.92
4	0	0	0	0	324.90
5	0	0	0	0	327.14
6	0	0	0	0	329.72

Table 15. The mean value and standard deviation of the optimal results.

Optimal Results	Strategy-1		Strategy-2		Strategy-3	
	Mean Value	Standard Deviation	Mean Value	Standard Deviation	Mean Value	Standard Deviation
θz_1 [°]	0	0	0	0	0	0
θz_2 [°]	120.01	0.0147	142.26	1.0617	0	0
θz_3 [°]	117.20	0.7563	45.07	0.0709	0	0
θz_4 [°]	121.67	0.8165	30.04	0.0662	0	0
Unbalance [g·mm]	181.69	0.6631	402.52	1.0800	326.57	1.1011

Table 16. The optimal results with considering the distributed screw holes of each component.

Strategy	θz_1 [°]	θz_2 [°]	θz_3 [°]	θz_4 [°]	Unbalance [g·mm]
1	0	120(4 × 30)	105(7 × 15)	120(4 × 30)	189.68
2	0	150(5 × 30)	60(4 × 15)	60(2 × 30)	403.07
3	0	0	0	0	320.65

The four-stage rotor was assembled according to the above three optimization results, and the unbalance of the assemblies was measured by a dynamic balancing machine further. The dynamic balancing machine was manufactured by Shanghai Shenzhong Co., Ltd. (Shanghai, China), and its minimum residual unbalance reaches 0.5 g·mm/kg. The experimental device was shown in Figure 10, and the corresponding results of the experiments were shown in Table 17.

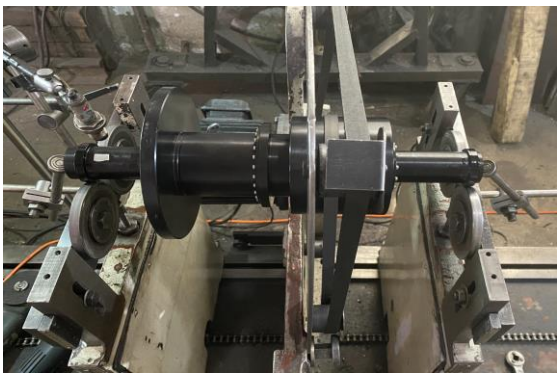

Figure 10. Measurement of the unbalance of the four-stage rotor.

Table 17. The results of three experiments.

Strategy	θz_1 [°]	θz_2 [°]	θz_3 [°]	θz_4 [°]	Unbalance [g·mm]
1	0	120(4 × 30)	105(7 × 15)	120(4 × 30)	184.6
2	0	150(5 × 30)	60(4 × 15)	60(2 × 30)	404.1
3	0	0	0	0	325.4

5. Results and Discussion

Comparing the calculated unbalance in Table 16 and the measured results in Table 17, the simulation results were in good agreement with the experimental results. As shown in Table 17, when the θz_2, θz_3, and θz_4 were 120°, 105°, and 120°, respectively (i.e., the calibrated screw holes of the LPC, HPC, and back shaft should rotate four, seven, and four distributed angles), the unbalance of the four-stage rotor reached the minimum value (184.6 g·mm). When the θz_2, θz_3, and θz_4 were 150°, 60°, and 60°, respectively (i.e., the calibrated screw holes of the LPC, HPC, and back shaft should rotate five, four, and two distributed angles), the unbalance of the four-stage rotor reached the maximum value (404.1 g·mm). When the θz_2, θz_3, and θz_4 were all 0° (i.e., the initial state), the unbalance of the four-stage rotor was 404.1 g·mm. Compared with the maximum unbalance and the initial unbalance, the minimum unbalance was notably reduced by 54.3% and 43.3%, respectively. These phenomena revealed that the proposed method of unbalance optimization for multi-stage rotor in this paper was effective.

The contents of the unbalance optimization method were mainly reflected in three aspects. First, an accurate assembly error propagation model is important to calculate the unbalance of a multi-stage rotor after assembly. The relevant simulation results in Section 3.1 showed that the assembly error propagation model developed in Section 2.1 was able to accurately predict the coordinates of any point in the assembled rotor. Moreover, the distribution of the screw holes of each single-stage rotor was not considered in the existing assembly error propagation models. In the actual assembly process of the multi-stage rotor, the assembly orientations of each single-stage rotor are finite and discrete. This is not simply to turn the continuous variables (0−180°) into the discrete variables (i.e., 180° divided by the number of the screw holes). In order to calculate the assembly cumulative error under any corresponding relationship of the screw holes of rotors at different stage, the sampling angles (φ_n) between the calibrated screw hole and the highest point of each single-stage rotor must be known. Therefore, the sampling angles were introduced into the error propagation model in our study to calculate the optimal corresponding relationship of each rotor. With comparison to the existing studies, the distribution of the screw holes of rotors at different stages was directly introduced into the model for the first time, which increases the suitability for guidance on actual assemblies.

The second aspect is concerned with the selection and calculation of the assembly datum for unbalance optimization. Considering the actual operating conditions of dynamic balancing for a rotor, two-plane unbalance measured by the dynamic balancing machine must be perpendicular to the axis of rotation of the measured rotor. Such an axis of rotation is simply a line connecting the midpoints of the journals of the front and back shaft. In current studies, the assembly datum for calculating unbalance of a multi-stage rotor was selected as the same as the measured datum for geometric parameter. It is clearly unreasonable that the simulated assembly axis is inconsistent with the axis of rotation of the dynamic balancing test. In addition, the results of the simulation are not comparable with the results of the experiment. In this study, we solved the problem by selecting the "orientation-varying axis" in Figure 3 as the assembly datum for unbalance optimization. The proposed assembly datum can ensure the constraint conditions of the unbalance optimization have good consistency with those of the dynamic balance test.

In terms of algorithm optimization, the bionics algorithm is now seldom applied in assembly optimization. Here, a GA was employed to achieve the optimal matching of assembly orientations for rotors at different stages. Such a strategy is applicable not only to the optimization of continuous angles but also to the optimization of discrete angles in the presence of screw holes for assembly.

6. Conclusions

Unbalance caused by improper assembly is the main reason for vibration faults in multi-stage rotors. A method is urgently needed to not only predict the state of a multi-stage rotor after assembly, but also to find the optimal matching relationship of a rotor

at different stages to minimize the unbalance of the rotor. In this study, we developed an unbalance optimization method of a multi-stage rotor based on an assembly error propagation model. The main contributions of this study can be summarized as follows:

1. An accurate assembly error propagation model was developed to calculate the coordinates of any point in a rotor at different stages after assembly. The alignment process and distribution of the screw holes of adjacent rotors were considered in this model for the first time.
2. A new assembly datum for unbalance optimization was proposed to ensure consistency with the actual conditions of the dynamic balance test.
3. Unbalance optimization of a multi-stage rotor was achieved using a GA. Additionally, the optimal assembly orientations of rotors at different stages were also identified.

Author Contributions: Conceptualization, Y.C. and J.C.; methodology, Y.C.; software, Y.C.; validation, Y.C.; formal analysis, Y.C.; investigation, Y.C.; resources, J.C.; data curation, Y.C.; writing—original draft preparation, Y.C.; writing—review and editing, Y.C.; visualization, Y.C.; supervision, X.S.; project administration, J.C.; funding acquisition, J.C. All authors have read and agreed to the published version of the manuscript.

Funding: This research was funded by the Outstanding Youth Project of Natural Science Foundation of Heilongjiang Province, Grant JQ2019E002. The authors are grateful for the financial support.

Institutional Review Board Statement: Not applicable.

Informed Consent Statement: Not applicable.

Data Availability Statement: Not applicable.

Acknowledgments: The authors acknowledge Cui, S. In the College of Mechanical Engineering, Tianjin University of Science and Technology for the active support of the research.

Conflicts of Interest: The authors declare no conflict of interest.

References

1. Ding, S.; Zheng, X.; Bao, J.; Zhang, J. A comprehensive study of three dimensional deviation analysis methods for aero-engine rotors assembly. *IOP Conf. Ser. Mater. Sci. Eng.* **2019**, *688*, 033039. [CrossRef]
2. Qin, Z.; Han, Q.; Chu, F. Bolt loosening at rotating joint interface and its influence on rotor dynamics. *Eng. Fail. Anal.* **2016**, *59*, 456–466. [CrossRef]
3. Wang, H.; Ge, Q. Aero structural assembly deformation prediction considering drilling-induced stresses. *J. Aerosp. Eng.* **2015**, *28*, 04015007. [CrossRef]
4. Wang, M.; Han, Q.; Wen, B. Modal characteristics and unbalance responses of fan rotor system with flexible support structures in aero-engine. *Proc. Inst. Mech. Eng. Part G J. Aerosp. Eng.* **2017**, *231*, 1686–1705. [CrossRef]
5. Hu, X.; Gao, F.; Cui, C. Analysis of mass unbalance torque on a spinning superconducting rotor. *IEEE Trans. Appl. Supercond.* **2013**, *24*, 3600204. [CrossRef]
6. Ercoli, L.; La, M.S. The development of a dynamic balancing machine. *Int. J. Mech. Eng. Educ.* **1998**, *26*, 149–155. [CrossRef]
7. Khazali, A.; Hisham, A.H.; Askari, M.R. The experimental analysis of vibration monitoring in system rotor dynamic with validate results using simulation data. *Isrn Mech. Eng.* **2014**, *2012*, 1–17. [CrossRef]
8. Hussain, T.; Yang, Z.; Popov, A.A. Straight-build assembly optimization: A method to minimize stage-by-stage eccentricity error in the assembly of axisymmetric rigid components (two-dimensional case study). *J. Manuf. Sci. Eng.* **2011**, *133*, 031014. [CrossRef]
9. Hussain, T.; Yasinshaikh, G.; Shaikh, S.A. Variation propagation control in straight-build assemblies: 2d case study. *Mehran Univ. Res. J. Eng. Technol.* **2013**, *32*, 71–80.
10. Yang, Z.; Hussian, T.; Popov, A.A. A comparison of different optimization techniques for variation propagation control in mechanical assembly. *IOP Conf.* **2011**, *26*, 012017. [CrossRef]
11. Yang, Z.; Hussian, T.; Popov, A.A. Novel optimization technique for variation propagation control in an aero-engine assembly. *Proc. Inst. Mech. Eng. Part B J. Eng. Manuf.* **2010**, *225*, 100–111. [CrossRef]
12. Hussain, T.; Mcwilliam, S.; Popov, A.A. Geometric error reduction in the assembly of axis-symmetric rigid components: A two-dimensional case study. *Proc. Inst. Mech. Eng. Part B J. Eng. Manuf.* **2012**, *226*, 1259–1274. [CrossRef]
13. Yang, Z.; Popov, A.A.; Mcwilliam, S. Variation propagation control in mechanical assembly of cylindrical components. *J. Manuf. Syst.* **2012**, *31*, 162–176. [CrossRef]
14. Yang, Z.; Popov, A.A.; Mcwilliam, S.; Hussian, T. Dimensional variation propagation analysis in straight-build mechanical assemblies using a probabilistic approach. *J. Manuf. Syst.* **2013**, *32*, 348–356. [CrossRef]

15. Jin, S.; Ding, S.; Li, Z. Point-based solution using Jacobian-Torsor theory into partial parallel chains for revolving components assembly. *J. Manuf. Syst.* **2017**, *46*, 46–58. [CrossRef]
16. Sun, C.; Li, C.; Liu, Y. Prediction method of concentricity and perpendicularity of aero engine multistage rotors based on PSO-BP neural network. *IEEE Access* **2019**, *7*, 132271–132278. [CrossRef]
17. Wang, L.; Sun, C.; Tan, J. Improvement of location and orientation tolerances propagation control in cylindrical components assembly using stack-build assembly technique. *Assem. Autom.* **2015**, *34*, 358–366. [CrossRef]
18. Sun, W.; Li, T.; Yang, D. Dynamic investigation of aeroengine high pressure rotor system considering assembly characteristics of bolted joints. *Eng. Fail. Anal.* **2020**, *112*, 104510. [CrossRef]
19. Piskin, A.; Aktas, H.E.; Topal, A. Rotor balancing with turbine blade assembly using ant colony optimization for aero-engine applications. *Int. J. Turbo Jet-Engines* **2017**, *8*, 0060. [CrossRef]
20. Liu, Y.; Zhang, M.; Sun, C. A method to minimize stage-by-stage initial unbalance in the aero engine assembly of multistage rotors. *Aerosp. Sci. Technol.* **2018**, *85*, 270–276. [CrossRef]
21. Sun, C.; Liu, Z.; Liu, Y. An adjustment method of geometry and mass centers for precision rotors assembly. *IEEE Access* **2019**, *7*, 169992–170002. [CrossRef]
22. Yang, X.S. *Nature-Inspired Meta-Heuristic Algorithms*; Luniver Press: Beckington, UK, 2008; pp. 314–322.